

## LLCL-Filtered Grid Converter with Improved Stability and Robustness

Min, Huang; Wang, Xiongfei; Loh, Poh Chiang; Blaabjerg, Frede

*Published in:*  
I E E E Transactions on Power Electronics

*DOI (link to publication from Publisher):*  
[10.1109/TPEL.2015.2467185](https://doi.org/10.1109/TPEL.2015.2467185)

*Publication date:*  
2016

[Link to publication from Aalborg University](#)

*Citation for published version (APA):*  
Min, H., Wang, X., Loh, P. C., & Blaabjerg, F. (2016). LLCL-Filtered Grid Converter with Improved Stability and Robustness. *I E E E Transactions on Power Electronics*, 31(5), 3958 - 3967.  
<https://doi.org/10.1109/TPEL.2015.2467185>

### General rights

Copyright and moral rights for the publications made accessible in the public portal are retained by the authors and/or other copyright owners and it is a condition of accessing publications that users recognise and abide by the legal requirements associated with these rights.

- Users may download and print one copy of any publication from the public portal for the purpose of private study or research.
- You may not further distribute the material or use it for any profit-making activity or commercial gain
- You may freely distribute the URL identifying the publication in the public portal -

### Take down policy

If you believe that this document breaches copyright please contact us at [vbn@aub.aau.dk](mailto:vbn@aub.aau.dk) providing details, and we will remove access to the work immediately and investigate your claim.

# LLCL-Filtered Grid Converter with Improved Stability and Robustness

Min Huang, *Student Member, IEEE*, Xiongfei Wang, *Member, IEEE*, Poh Chiang Loh, and Frede Blaabjerg, *Fellow, IEEE*

**Abstract**— *LLCL-filter has been proven to introduce more filtering at the converter switching frequency, while using smaller passive components. However, like other higher order filters, it introduces resonance to the grid when used with a grid converter. Its stability and robustness are also affected by grid impedance variations, making its design more challenging. To address these concerns, a new parameter design method for LLCL-filter has been formulated in the paper, which when enforced, guarantees robust and stable grid current control regardless of how the grid conditions change. It is thus an enhanced method even with no damping added to the grid converter. The method has been applied to the development of an LLCL-filter for testing in the laboratory with a 5-kW, 400-V, and 50-Hz grid converter. The method can also be applied to the lower order LCL-filter with only a slight modification needed.*

**Index Terms**— *Filter design, resonance, robustness, stability, delay.*

## I. INTRODUCTION

**M**OST modern sources are connected to the power grid through grid-connected converters, which with the advancement of semiconductor technology, are almost always switching at high frequencies. Such switching, however, introduces harmonics and rapid state transitions, which are usually not desired by the grid. It is therefore common to place a low-pass power filter between each converter and the grid for attenuating high frequency harmonics in the injected grid current [1], [2]. The filter introduced can be of different types like shown in Fig. 1. The simplest consists of only an inductor  $L$  like in Fig. 1(a). Its gain roll-off is however only  $20\text{ dB/dec}$ , which may not be sufficient at high frequencies. One solution is to use a larger  $L$  at the expense of poorer dynamic and higher loss. It is therefore not generally recommended. Alternatively, the higher order  $LCL$ -filter shown in Fig. 1(b) can be used. Its higher gain roll-off of  $60\text{ dB/dec}$  provides better attenuation even with a smaller total inductance used. The resulting filter can therefore be much cheaper and hence more attractive at the kilowatt level [3].

The required inductance and capacitance can further be reduced by replacing the middle  $C$  branch of an  $LCL$ -filter with a series  $LC$  trap, as shown in Fig. 1(c). The modified filter has been named as the  $LLCL$ -filter in [4]-[8], which when compared with the  $LCL$  filter, has an extra small inductor  $L_f$

added. This inductor, together with the re-notated capacitor  $C_f$ , is usually tuned to resonate at the converter switching frequency. Harmonics around the switching frequency will then flow through the low impedance path formed by  $L_f$  and  $C_f$ , rather than enter the grid. The resulting  $LLCL$ -filter will hence be equally effective even with smaller total inductance and capacitance used. The same principle can obviously be repeated by adding more  $LC$  traps tuned at other dominant harmonic frequencies, like shown in Fig. 1(d) [9]. Although the total passive component sizes can be reduced even more, the complexity introduced may not be encouraged. One particular concern, for example, is the interaction among multiple trap filters found in either one or multiple nearby converters.

The number of trap per filter is thus commonly kept at one, giving rise to the fourth order  $LLCL$ -filter. Like other higher order filters, the challenge is then to damp accompanied resonance, which if not ensured, may destabilize the grid.  $LLCL$ -filter and other higher order filters are thus commonly damped by adding physical resistors or actively modifying their converter control [10]-[16]. Adding a damper is however not strictly necessary, as proven in [10] for an  $LCL$ -filter and [7] for an  $LLCL$ -filter. These references, in particular, conclude that for both filters, damping is not required if their resonance frequencies are placed above one-sixth of the sampling frequency ( $f_s / 6$ ). Such intentional placement is however not very robust since a change in grid impedance may accidentally push the resonance peaks below  $f_s / 6$  [17]-[20].

Design methods and criteria for  $LLCL$ -filter when used with a grid converter have therefore surfaced in [4] and [6] with each criterion normally defined for setting one filter component [3]. For example, the converter-side inductance is usually determined by the maximum permitted current ripple flowing through the converter, while the filter capacitance is usually set according to the amount of reactive power permitted. The grid-side inductance can then be determined based on the level of harmonic attenuation demanded [6], [21]. The final objective is to have high attenuation, while using the same or smaller total passive reactance [16]. No doubt, these are important requirements, but will only be meaningful if stability and robustness can be guaranteed first. Simultaneous achievement of stability and robustness has however neither been discussed in [4] nor [6], where existing design methods for  $LLCL$ -filter are documented.

It is therefore important to re-evaluate the design of a  $LLCL$ -filtered converter carefully, before it can be realized

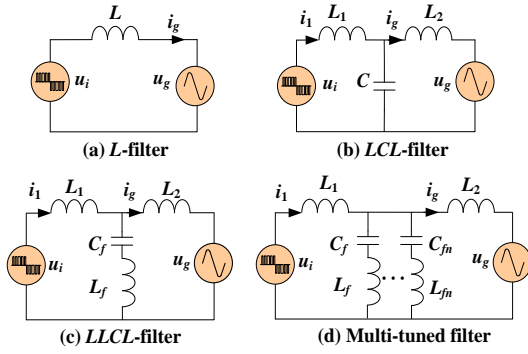


Fig. 1. Topologies of different power filters.

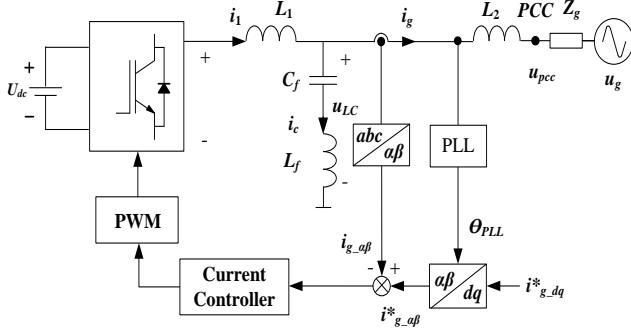


Fig. 2. *LLCL*-filtered converter with a single control loop.

stably and robustly. In other words, the resulting converter must work properly with the grid (stability) regardless of usual changes expected from the grid (robustness). This challenge has been demonstrated as attainable in the paper by applying a newly proposed design method for *LLCL*-filter. The method can similarly be applied to an *LCL*-filter, but with a slight limitation to be explained in the paper. The method has been tried with its designed *LLCL*-filter tested with a 5-kW, 400-V, and 50-Hz grid converter. Results obtained have shown a robustly stable converter operating with a wide range of grid impedance conditions.

## II. MODELING OF *LLCL*-FILTERED GRID CONVERTER

### A. System Description

Fig. 2 illustrates a grid converter powered by dc voltage  $U_{dc}$  and filtered by a *LLCL*-filter comprising  $L_1$ ,  $L_2$ ,  $L_f$  and  $C_f$ . The converter output voltage and current are notated as  $u_i$  and  $i_1$ , whose values are determined by only a single feedback loop for regulating grid current  $i_g$  synchronized with voltage  $u_{LC}$  across the  $L_f C_f$  trap. The single feedback loop with only a current controller is realized in the stationary  $\alpha\beta$ -frame. Between voltage  $u_{pcc}$  at the point-of-common-coupling (PCC) and grid voltage  $u_g$  is the grid impedance  $Z_g$ , whose value is normally changing. The challenge is thus to stabilize the single grid current control loop regardless of how the grid impedance changes. For that, Fig. 3 is referred to, where block diagram for illustrating the control loop is shown, together with impedances  $Z_{L1}$ ,  $Z_{LC}$  and  $Z_{L2}$  for  $L_1$ , the middle  $L_f C_f$  trap and  $L_2$ , respectively. Other parameters of the system are summarized in Table I.

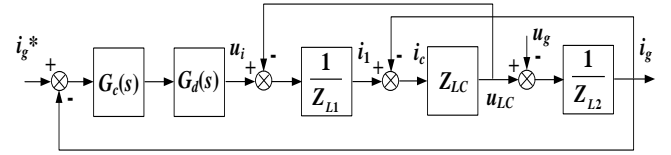


Fig. 3. Grid current control of an *LLCL*-filtered converter.

TABLE I SYSTEM PARAMETERS

Symbol	Definition	Value
$U_{dc}$	DC link voltage	730 V
$U_g$	Grid voltage	400 V
$f_o$	Grid frequency	50 Hz
$T_s = 1/f_s$	Sampling period	100 $\mu$ s
$f_{sw} = f_s$	Switching frequency	10 kHz

Also included in Fig. 3 are  $G_c(s)$  as a current controller for tracking reference  $i_g^*$ , and  $G_d(s)$  for representing computational and modulation delays. Controller  $G_c(s)$  can be a proportional-resonant (PR) controller with multiple resonant peaks at low-order harmonic frequencies. Its transfer function is thus given as:

$$G_c(s) = K_p + \sum_{h=1,5,7,11,13} \frac{K_{ih}s}{s^2 + (\omega_0 h)^2} \quad (1)$$

where  $\omega_0 = 2\pi f_o$  is the fundamental angular frequency,  $K_p$  is the proportional gain, and  $K_{ih}$  is the resonant gain at harmonic order  $h$ . Delay  $G_d(s)$  is, on the other hand, commonly expressed as:

$$G_d(s) = e^{-\lambda T_s s} \quad (2)$$

where  $T_s = 1 / f_s$  are the sampling period and frequency, respectively, and  $\lambda$  is the delay time normalized with  $T_s$ .

### B. Norton Equivalent Model

Fig. 4 shows the Norton equivalent model of the *LLCL*-filtered grid converter with grid current control [20]. Also shown are grid capacitance  $C_g$  (in case of cable) and inductance  $L_g$ , which together, form  $Z_g$ . Parameters of the model like its closed-loop gain  $G_{c1}$  and output admittance  $G_{c2}$  are obtained from Fig. 3 by first writing down their common open-loop transfer functions from  $i_g$  to  $u_i$  and  $i_g$  to  $u_{pcc}$ , as given in (3) and (4) below.

$$G_1 = \left. \frac{i_g}{u_i} \right|_{u_{pcc}=0} = \frac{Z_{CL}}{Z_{L1}Z_{L2} + Z_{L1}Z_{CL} + Z_{L2}Z_{CL}} \quad (3)$$

$$G_2 = \left. \frac{i_g}{u_{pcc}} \right|_{u_i=0} = \frac{Z_{L1} + Z_{CL}}{Z_{L1}Z_{L2} + Z_{L1}Z_{CL} + Z_{L2}Z_{CL}} \quad (4)$$

The open-loop gain  $T$ , closed-loop gain  $G_{c1}$  and closed-loop output admittance  $G_{c2}$  of the single-loop grid current control can then be determined as:

$$T = G_c G_d G_1 \quad (5)$$

$$G_{c1} = \frac{T}{1+T} \quad (6)$$

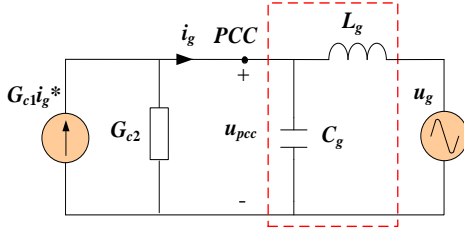


Fig. 4. Norton equivalent model of grid-current-controlled converter.

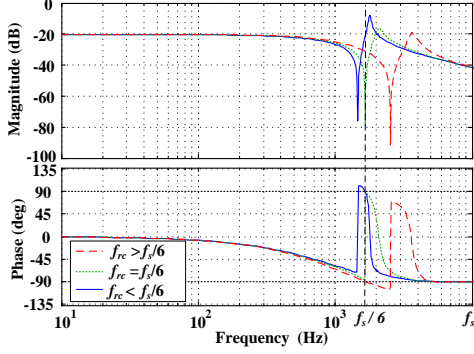


Fig. 5. Bode plots of closed-loop output admittance  $G_{c2}$  with different  $f_{rc}$  values.

$$G_{c2} = \frac{G_2}{1+T} = 1 / \left( \frac{1}{G_2} + \frac{T}{G_2} \right) \quad (7)$$

According to Fig. 4,  $i_g$  can next be expressed as (8), to which (6) and (7) can be substituted to arrive at a final expression for representing the grid current control scheme. The expression will show that stability of the scheme is affected by resonance at frequency  $\omega_r$  ( $\omega_r = 2\pi f_r$ ) computed with (9).

$$i_g = G_{c1} i_g^* - G_{c2} u_{pcc} \quad (8)$$

$$\omega_r = \frac{1}{\sqrt{\left( \frac{L_1(L_2 + L_g)}{L_1 + L_2 + L_g} + L_f \right) C_f}} \quad (9)$$

### III. STABILITY AND ROBUSTNESS

#### A. Concept of Passivity

To be passive, a linear continuous system  $G(s)$  must satisfy the following two requirements at frequency  $\omega$  [22].

- $G(s)$  has no right-half-plane (RHP) poles, and
- $\text{Re}\{G(j\omega)\} \geq 0 \Leftrightarrow \arg\{G(j\omega)\} \in [-90^\circ, 90^\circ], \forall \omega > 0$ .

They include all  $RLC$  components, meaning the grid impedance shown in Fig. 4 is naturally passive. Stability of the system in Fig. 4 is thus solely decided by the closed-loop output admittance  $G_{c2}$  of the converter, which must hence also be passive [20]. Passivity of  $G_{c2}$  is however not always possible especially with delay  $G_d$  considered like in Fig. 3. To illustrate, the term of  $G_{c2}$  in (7) that depends on delay is written as follows.

$$G_{2T} = \frac{G_2}{T} = \frac{1 - (L_1 + L_f)C_f\omega^2}{K_p(1 - C_fL_f\omega^2)} e^{j\lambda T_s\omega} \quad (10)$$

$$= \frac{1 - (L_1 + L_f)C_f\omega^2}{K_p(1 - C_fL_f\omega^2)} [\cos(\lambda T_s\omega) + j\sin(\lambda T_s\omega)]$$

where only the proportional gain of  $G_c(s)$ ,  $K_p$ , is considered in the analyses below, since the resonant controller gains are here designed to compensate the steady-state errors at the fundamental and low-order harmonic frequencies [12], which have little effect about the system resonance frequency [10].

Further defining  $f_{rc}$ ,  $f_{sw}$  ( $= f_s$ , if the switching and sampling frequencies are set equal) and  $f_{rd}$  according to (11) to (13), the real part of (10) can be simplified as (14).

$$f_{rc} = \frac{1}{2\pi\sqrt{(L_1 + L_f)C_f}} \quad (11)$$

$$f_{sw} = 1 / (2\pi\sqrt{L_f C_f}) \quad (12)$$

$$f_{rd} = \frac{f_s}{4\lambda} \quad (13)$$

$$\text{Re}\{G_{2T}\} = \frac{1 - (\omega/(2\pi f_{rc}))^2}{K_p(1 - (\omega/(2\pi f_s))^2)} \cos\left(\frac{\pi}{2} \times \frac{\omega}{(2\pi f_{rd})}\right) \quad (14)$$

Under normal operation up to the Nyquist frequency  $\omega < \pi f_s$ , the denominator of (14) will always be positive. The polarity of (14) is therefore solely determined by the two terms in the numerator, from which the following three observations can be drawn [20].

- By setting  $f_{rc} < f_{rd}$ , (14) will be negative in the range of  $f_{rc} < \omega / (2\pi) < f_{rd}$ .
- By setting  $f_{rd} < f_{rc}$ , (14) will be negative in the range of  $f_{rd} < \omega / (2\pi) < f_{rc}$ .
- By setting  $f_{rc} = f_{rd}$ , (14) will always be positive.

The third condition, in turn, causes (10) and (7) to be always positive, and hence a robustly passive output admittance  $G_{c2}$  to always appear across the converter model shown in Fig. 4. The overall system is thus always stable regardless of how the grid impedance changes. This conclusion can also be deduced from Bode plots of  $G_{c2}$  drawn with those system values specified in Table I, but with different  $f_{rc}$  values. The traces obtained are shown in Fig. 5 for the common case of  $\lambda = 1.5$ , and hence  $f_{rd} = f_s / 6$  according to (13). The task is then to identify regions, where  $G_{c2}$  becomes negative, or has phase exceeding  $90^\circ$  or falling below  $-90^\circ$ . The identification again leads to the following three summarized observations.

- Phase greater than  $90^\circ$  only happens between  $f_{rc}$  and  $f_s / 6$  if  $f_{rc} < f_s / 6$ .
- Phase smaller than  $-90^\circ$  only happens between  $f_s / 6$  and  $f_{rc}$  if  $f_s / 6 < f_{rc}$ .
- Phase will always be between  $-90^\circ$  and  $90^\circ$  if  $f_{rc} = f_s / 6$ .

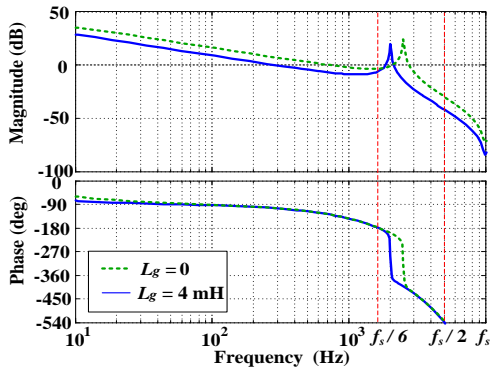


Fig. 6. Bode plots of open-loop control gain  $T$  with different  $L_g$  values.

As anticipated, the optimal condition is still the equality of  $f_{rc} = f_{rd}$  if both stability and robustness are to be ensured simultaneously.

### B. Criterion for Stability and Robustness without Damping

For most digitally controlled systems, delay of  $\lambda = 1.5$  is common. From (13),  $f_{rd}$  is then  $f_s / 6$ , which is also the frequency derived in [7] for another aspect related to an *LLCL*-filtered converter. To be more precise, it has been proven in [7] that if the system resonance frequency  $f_r$  in (9) is placed above  $f_s / 6$ , no damping is needed for stabilizing the *LLCL*-filtered converter. This can be seen from Fig. 6, where the frequency responses of open-loop gain  $T$  in (5) without damping have been plotted. The system is clearly stable since its phase crosses  $-180^\circ$  before the resonance peak at  $f_r$ , especially for the case of  $L_g = 0$ . As  $L_g$  increases to 4 mH, the system is still stable, but its resonance peak has moved closer to  $f_s / 6$ . This movement will continue as  $L_g$  increases further until the resonance peak eventually falls below  $f_s / 6$ . When that happens, the system must be stabilized by an explicitly added damper, which [8] has discussed different possibilities for a *LLCL*-filtered converter operated with different sampling rates. The study in [7] therefore lacks robustness, which has now been solved in this paper by deriving the optimal equality of  $f_{rc} = f_{rd} = f_s / 6$ .

The equality is however tough to satisfy precisely since  $f_{rc}$  depends on filter parameters  $L_1$ ,  $L_f$  and  $C_f$ , which can still vary even though not as much as the grid impedance. A more relaxed condition can therefore be helpful, and is provided in (15) with the system resonance frequency  $f_r$  included.

$$f_{rd} = f_s / 6 \leq f_{rc} < f_r \quad (15)$$

No doubt and according to Section III(A),  $f_{rc}$  higher than  $f_s / 6$  in (15) will create an interval ( $f_s / 6 < \omega / (2\pi) < f_{rc}$ ), within which the real part of the converter output admittance  $G_{c2}$  in Fig. 4 will become negative, and hence no longer passive. This interval will however never be entered by the system resonance frequency  $f_r$ , as easily proved by comparing the denominators of (9) and (11), while noting that  $\frac{L_1(L_2 + L_g)}{L_1 + L_2 + L_g} = L_1 / (L_2 + L_g) < L_1$ . Resonance frequency  $f_r$  in (9) will therefore always be higher than  $f_{rc}$  in (11) regardless

of how  $L_g$  varies. Condition (15) is thus a strong design criterion newly formulated for *LLCL*-filter, which upon ensured, guarantees both stability and robustness even with no damping added to the converter. The same criterion in (15) can also be applied to an *LCL*-filter upon setting  $L_f = 0$  in (9) to (11). It should however be noted that for an *LCL*-filter, keeping its resonance frequency  $f_r$  above  $f_s / 6$  will significantly degrade its harmonic attenuation around the switching frequency. Its attenuation will, in fact, approach the level of a large first-order *L*-filter [10]. This problem is however not experienced by an *LLCL*-filter because of its intentionally tuned  $L_f C_f$  trap added for removing harmonics around the switching frequency.

## IV. PARAMETER DESIGN PROCEDURE

When designing a power filter, a base impedance of its applied system should preferably be defined like in (16) using values from Table I. The base impedance can then be used for computing the base inductance and capacitance according to (17) and (18).

$$Z_b = \frac{U_g^2}{P_o} = 32 \Omega \quad (16)$$

$$C_b = \frac{1}{\omega_o Z_b} = 100 \mu\text{F} \quad (17)$$

$$L_b = \frac{Z_b}{\omega_o} = 102 \text{ mH} \quad (18)$$

where  $U_g = 400$  V is the base line-to-line RMS voltage,  $\omega_o = 2\pi \times 50$  rad / s is the base grid frequency, and  $P_o = 5$  kW is the base rated active power. With these base expressions defined, the following parameter design procedure can be formulated for an *LLCL*-filter with all constraints discussed in [3], [23] and [24] taken into consideration. The procedure is, no doubt, close to those mentioned in [25]-[28], but unlike them, the procedure presented here has included (15), which as explained earlier, is a newly formulated criterion needed for guaranteeing both stability and robustness even with no damping added to the converter. It is therefore a stronger design procedure, which has not been discussed in the literature.

### A. Converter-Side Inductance $L_1$

Being placed at the converter immediate output,  $L_1$  must be sized such that its peak-to-peak current ripple at the converter switching frequency  $f_s$  does not exceed  $\alpha$  times of its peak rated current  $I_{ref}$ . According to [28],  $\alpha$  can be up to 60% for an *LLCL* filter with better harmonic attenuation at the converter switching frequency. Based on the derivations presented in [4] and [28],  $L_1$  can then be sized with  $L_1 = U_{dc} / (8f_s \alpha I_{ref})$ , where  $U_{dc}$  is the dc-link voltage marked in Fig. 2. Substituting values from Table I and a more conservative  $\alpha$  of 49% eventually gives  $L_1 = 1.8$  mH for the experimental filter implemented for testing.

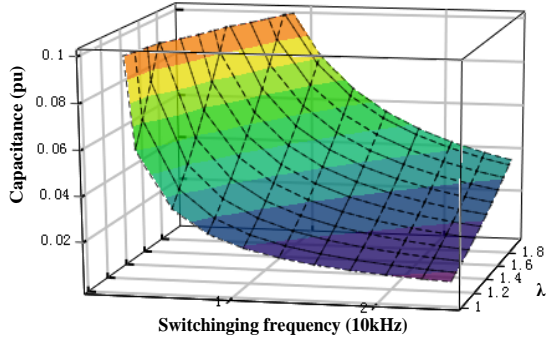


Fig. 7. Capacitance variation with switching frequency and delay  $\lambda$ .

### B. Capacitance $C_f$

From (11),  $C_f$  can be computed after deciding on  $L_1$ ,  $f_s = 1/(2\pi\sqrt{L_f C_f})$  and a value for  $f_{rc} \geq f_s / (4\lambda)$  ( $= f_s / 6$  if  $\lambda = 1.5$ ) that satisfies the robust stability criterion presented in (15). Value for  $C_f$  is therefore not unique, but varies with parameters used for computing it. This is demonstrated in Fig. 7, where  $C_f$  in *p.u.* is shown to increase with smaller  $f_s$  and bigger  $\lambda$ . A further constraint should therefore be introduced, which in most cases, is to select  $C_f$  such that the maximum power factor at rated power is less than 5%. In terms of its base value,  $C_f$  is then constrained according to  $C_f \leq 5\% \times C_b$ , which for the implemented filter, is computed as  $4.9 \mu\text{F}$  with  $\lambda = 1.5$  and  $f_s = 10 \text{ kHz}$ .

### C. Inductance $L_f$

After deciding on  $C_f = 4.9 \mu\text{F}$ , inductance  $L_f = 52 \mu\text{H}$  can be computed immediately since they form a series trap at the converter switching frequency of  $f_s = 10 \text{ kHz}$ . The extent of attenuation introduced by the series trap is however influenced by its quality factor  $Q$  expressed in (19).

$$Q = \frac{1}{R_f} \sqrt{\frac{L_f}{C_f}} \quad (19)$$

$$n = \sqrt{\frac{L_f}{C_f}} \quad (20)$$

where  $R_f$  represents the combined equivalent series resistance of  $L_f$  and  $C_f$ . Quality factor  $Q$  therefore depends on both  $R_f$  and  $n$  defined in (20). Their influences on the series trap impedance are better illustrated in Fig. 8 and Fig. 9. Beginning with Fig. 8, it shows that the trap width can be broadened by decreasing  $n$ , and hence decreasing  $Q$ , without affecting the minimum attenuation achievable. It can therefore be helpful if sideband harmonics centered around the switching frequency are spread far apart. In contrast, Fig. 9 shows that the width of the trap is not significantly changed by increasing  $R_f$ , and hence decreasing  $Q$ . Rather, the minimum trap impedance is raised, which will cause attenuation to be not as effective. It is

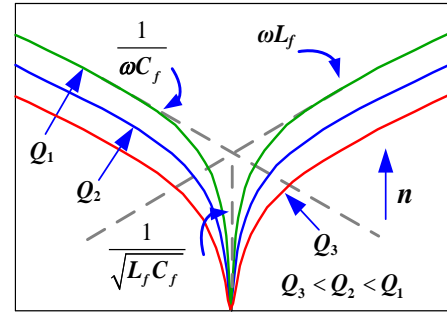


Fig. 8.  $LC$  trap impedance variation with different  $n$ .

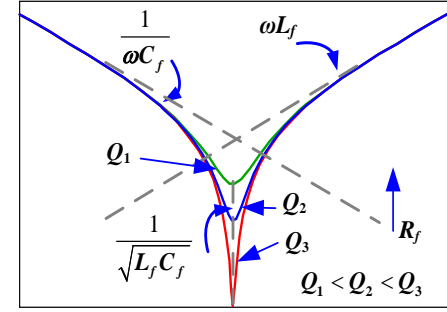


Fig. 9.  $LC$  trap impedance variation with different  $R_f$ .

therefore preferred to keep  $R_f$  low, especially when damping is not required after satisfying (15). The value of  $Q$  chosen should therefore be closer to 50 if the usual practical range of  $10 \leq Q \leq 50$  [28] is considered.

### D. Grid-Side Inductance $L_2$

Inductance  $L_2$  of the  $LLCL$ -filter is the final parameter to design. Its value can be comparably small since it carries no dominant harmonics around the switching frequency, which instead, have been diverted away by the middle  $L_f C_f$  trap. Inductance  $L_2$  therefore needs to attenuate only harmonics around the second integer multiple of the switching frequency to be lesser than 0.3% [6]. This is in accordance to the IEEE 519-1992 standard [29], where limits for different harmonic components and total harmonic distortion of the grid current have been defined in terms of the nominal grid fundamental current  $I_g$ . The limits are given in Table II, from which it is noted that all harmonics above the 35<sup>th</sup> order must be reduced below 0.3%. It is therefore appropriate to attenuate harmonics around the second integer multiple of the switching frequency to be lesser than 0.3% since they are above the 35<sup>th</sup> order. Based on this,  $L_2$  is chosen as 1.2 mH. The overall range of system resonance frequency  $f_r$  variation can then be computed using (9) by substituting the two probable extreme values of the grid inductance  $L_g$ . The lowest  $f_r$  computed will however still be higher than  $f_{rc}$  computed using (11). Explanation for that can be found in Section III (B). By further placing them ( $f_{rc}$  and  $f_r$ ) above  $f_s / 6$ , (15) will always be met, implying that the designed  $LLCL$ -filtered converter will always be robustly stable regardless of how  $L_g$  varies.

TABLE II MAXIMUM PERMITTED HARMONIC CURRENT DISTORTION IN PERCENTAGE OF CURRENT  $I_g$

Individual Harmonic Order $h$	$h < 11$	$11 \leq h < 17$	$17 \leq h < 23$	$23 \leq h < 35$	$35 < h$	THD
Percentage (%)	4.0	2.0	1.5	0.6	0.3	5.0

TABLE III FILTER PARAMETERS

Symbol	Definition	Case I	Case II
$L_1$	Inverter-side inductor	1.8 mH	1.8 mH
$L_2$	Grid-side inductor	1.2 mH	1.2mH
$L_f$	Resonant inductor	52 $\mu$ H	38 $\mu$ H
$C_f$	Capacitor	4.9 $\mu$ F	6.7 $\mu$ F
$f_r$	Resonant frequency ( $L_g = 0$ mH)	2.56 kHz	2.23 kHz
$f_{rc}$	Frequency	1.67 kHz	1.42 kHz

### E. Other Constraints

Where necessary, filter parameters computed from the earlier four subsections can be iterated, like in Fig. 10, to make sure that other converter and grid limitations are not breached. One of them is related to the total inductance ( $L_1 + L_2$ ) and its voltage drop, which if excessive, will significantly raise the minimum required dc-link voltage, and hence system loss. It is therefore advisable to limit ( $L_1 + L_2$ ) below 0.1 p.u.. Such limitation can be realized by increasing the converter switching frequency and / or capacitance  $C_f$ , as demonstrated in Fig. 11. Lowering of ( $L_1 + L_2$ ) must however not be too excessive since low-order harmonics in the grid current must be kept below the IEEE 519-1992 standard summarized in Table II.

The next issue to check is whether the system resonance frequency  $f_r$  is above ten times the line frequency and below the Nyquist frequency, which is half the sampling frequency  $f_s$ . The lower limit is for avoiding common low-order harmonics present in the grid, which in most cases, is not a concern since  $f_r$  has intentionally been placed above  $f_s / 6$ , as demanded by (15). The upper Nyquist limit can also safely be avoided by designing  $f_r$  in (9) to be smaller than the Nyquist frequency when  $L_g = 0$ . As  $L_g$  increases in a real grid,  $f_r$  will then shift towards the left and away from the Nyquist frequency, as understood from Fig. 6. Limitations imposed on the resonance range will therefore not likely be breached.

Another frequency range of interest is that related to  $f_{rc}$ , which in case of parameter drift, will deviate from its nominal value. The deviation can be computed by assuming a +5% change for  $C_f$ , and a  $\pm 2\%$  change for  $L_1$  and  $L_f$ , according to the industrial filter tolerances specified in [30]. Substituting these tolerances to (11) then results in  $f_{rc}$  varying between 96.9% and 103% of its nominal value  $f_{rc,nom}$ . The design using (15) must hence consider  $96.9\% \times f_{rc,nom}$  rather than  $f_{rc,nom}$ . The eventual parameters satisfying (15) and used for implementing the experimental LLCL-filter are given as Case I in Table III. For comparison, Case II designed without satisfying (15) is also given in the table. The non-optimized frequency relation of Case II is  $f_{rc} < f_s / 6 < f_r$ , which will gradually lead to

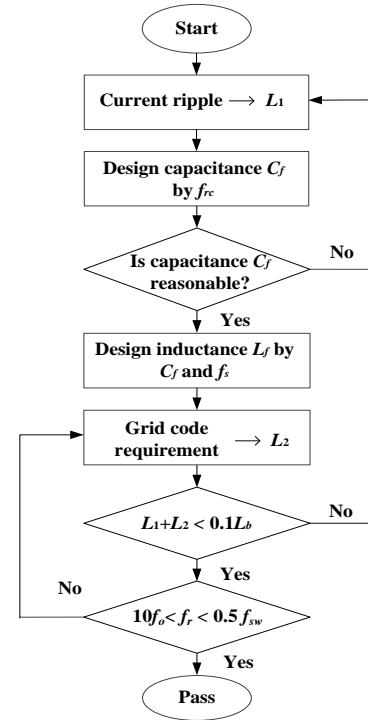


Fig. 10. Flow chart showing the parameter design procedure.

instability when  $f_r$  is pushed below  $f_s / 6$  by a sufficiently large grid inductance.

### F. Controller Design

The grid current is controlled by a PR controller  $G_c(s)$  with multiple resonant peaks at the 5<sup>th</sup>, 7<sup>th</sup>, 11<sup>th</sup> and 13<sup>th</sup> harmonics. Fig. 2 and Fig. 3 show the control scheme in the stationary  $\alpha\beta$ -frame, while (1) to (9) give their derived transfer functions in the  $s$ -domain. For digital implementation, the open-loop transfer function in (5) must further be discretized by applying a zero-order-hold (ZOH) transform to (3) to give (21) in the  $z$ -domain for analysis [10].

$$T(z) = K_p \cdot z^{-1} \cdot Z \left[ \frac{1 - e^{-sT_s}}{s} G_1 \right] \quad (21)$$

Stability of the grid-current-controlled converter can then be analyzed by drawing root loci using filter parameters summarized in Table III for Case I and Case II. Fig. 12(a) and (b) show the root loci drawn by increasing  $K_p$ , while keeping  $L_g = 0$  and the relative low resonant gain in (1) at  $K_{ih} = 500$ . The figures clearly show that for Case I, the maximum  $K_p$  is 19.8, while for case II, it is 14.8. The values chosen are thus  $K_p = 14.8$  for Case I and  $K_p = 10.5$  for Case II, based on the largest obtainable damping ratios.

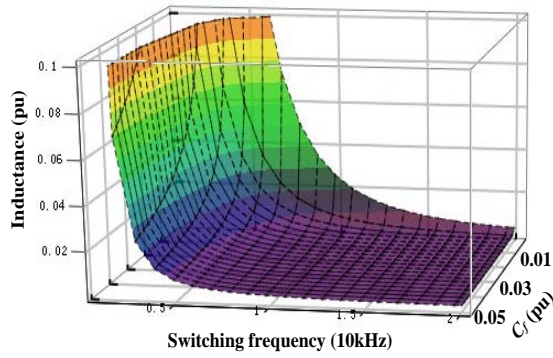
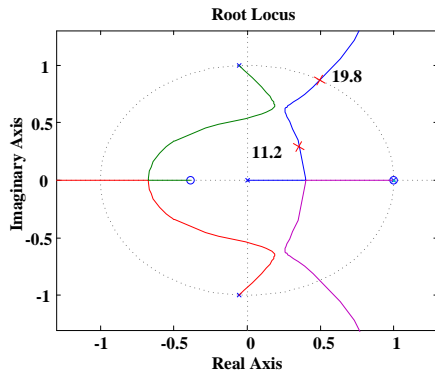
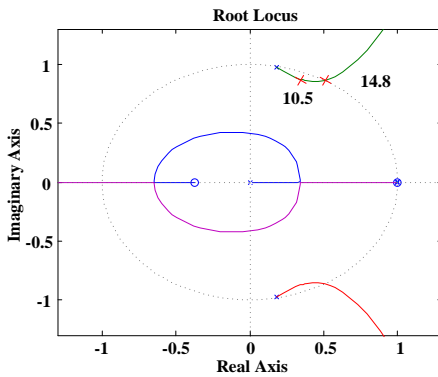


Fig. 11. Total inductance variation with capacitance and switching frequency.



(a)

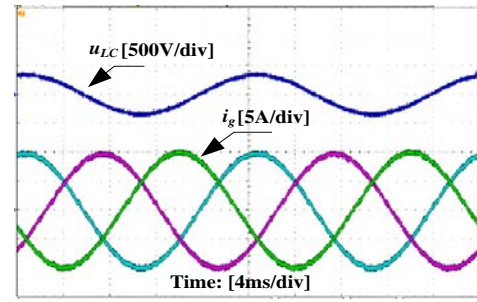


(b)

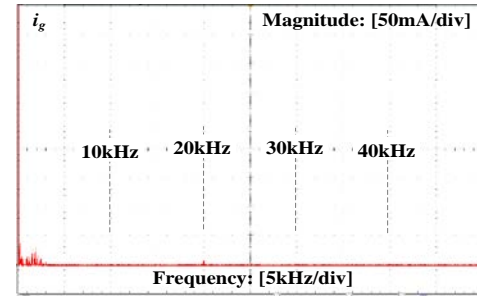
Fig. 12. Root loci of the grid-current-controlled converter when filtered by parameters from (a) Case I and (b) Case II without damping.

## V. EXPERIMENTAL RESULTS

The experimental setup consists of a 5-kW Danfoss FC302 converter tied to the grid through a transformer and an  $LLCL$ -filter. Power source to the converter is provided by a Delta Elektronika dc power supply, while its control in Fig. 2 and Fig. 3 is implemented with a dSPACE DS1007 controller platform. Parameters used for the experiment are summarized in Table I and III, where the latter includes Case I and Case II designed with and without (15) considered. With this setup and the designed controller, Fig. 13(a) shows the steady-state grid currents and voltage across the  $L_f C_f$  trap obtained with  $L_g = 0$  mH and those properly designed  $LLCL$  parameters of Case I. Fig. 13(b) shows the grid current spectrum, which clearly



(a)



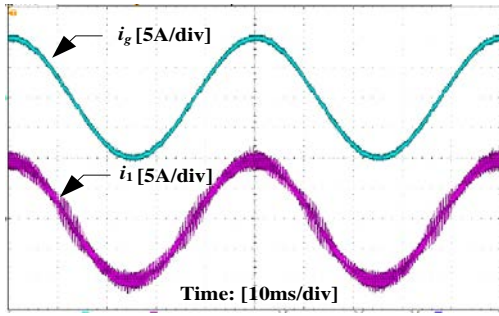
(b)

Fig. 13. Experimental (a) voltage across  $LC$  trap and grid currents, and (b) grid current spectrum obtained with properly designed  $LLCL$  parameters from Case I.

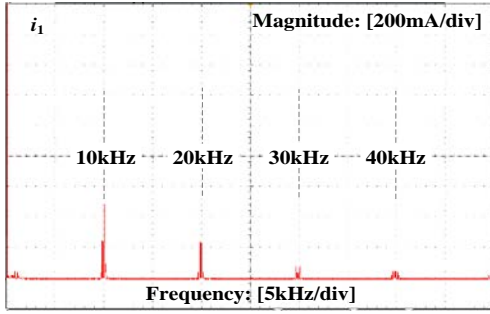
has dominant harmonics only at twice the switching frequency. This is expected since dominant harmonics at the switching frequency have been diverted away by the  $L_f C_f$  trap. Other lower order ( $17^{\text{th}}$ ,  $19^{\text{th}}$ ,  $23^{\text{th}}$  and  $25^{\text{th}}$ ) harmonics observed in the figure are caused by the grid background voltage harmonics, not compensated by the resonant terms of (1), which for the experiments, are set to  $h = 5, 7, 11$  and  $13$  only.

Fig. 14(a) next shows the grid- and converter-side currents with the properly designed  $LLCL$  parameters of Case I. Spectrum of the converter-side current is also given in Fig. 14(b), which clearly, has dominant harmonics at the switching frequency. This is expected since dominant harmonics at the switching frequency will only be removed after passing through the  $L_f C_f$  trap. They will therefore only be removed in Fig. 13(b), where the grid current spectrum has been plotted. The grid current responses during a step-transition from half to full load with grid inductance  $L_g = 0$  have also been shown in

Fig. 15(a) for Case I and Fig. 15(b) for Case II designed without considering (15). Both cases are dynamically comparable, even though Case I has a slightly less oscillatory response. Case I is however more robust as demonstrated by comparing Fig. 16(a) for Case I with Fig. 16(b) for Case II. Both figures show the same grid currents and voltage across the  $L_f C_f$  trap, but with  $L_g$  increased from 0 to 5 mH. The increase causes the resonance peak  $f_r$  to shift leftward, as understood from Fig. 6. The shift is however always above  $f_s / 6$  for Case I because of (15). Case I is thus robustly stable even with no passive and active damper used with the converter. Case II is, on the other hand, not robust since the higher  $L_g$  has shifted  $f_r$  below  $f_s / 6$ , which in general, can happen since (15) has not been ensured.

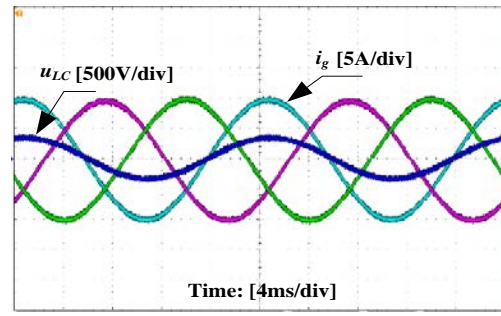


(a)

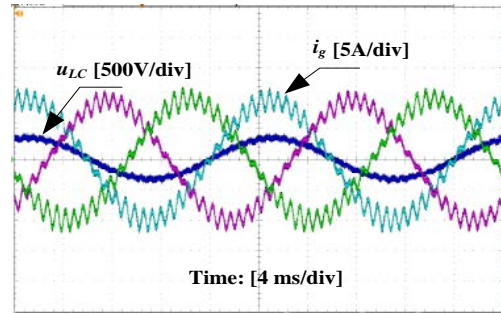


(b)

Fig. 14. Experimental (a) grid- and converter-side currents, and (b) converter-side current spectrum obtained with properly designed  $LLCL$  parameters from Case I.

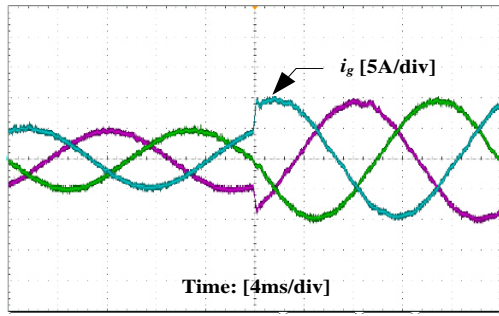


(a)

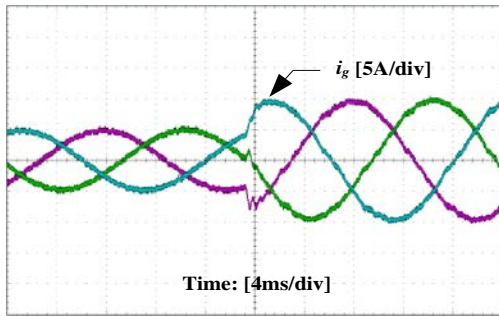


(b)

Fig. 16. Experimental voltage across  $LC$  trap and grid currents with the same  $L_g = 5\text{mH}$ , but different filter parameters from (a) Case I and (b) Case II.



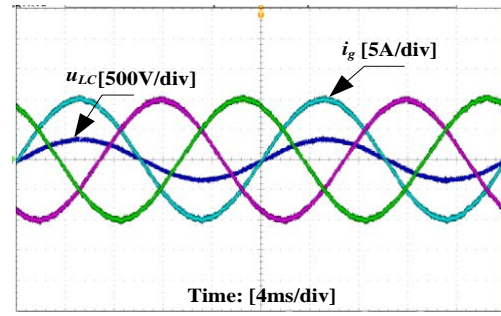
(a)



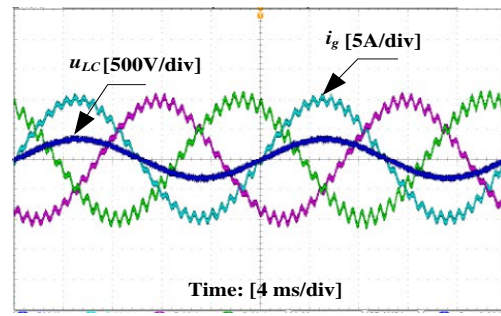
(b)

Fig. 15. Experimental grid currents during transition from half to full load with  $L_g = 0$  and filter parameters from (a) Case I and (b) Case II.

To further test the converter robustness with Case I,  $C_g$  in Fig. 4 is set to the finite value of  $6.7\ \mu\text{F}$ , while  $L_g$  is set to  $1.8\ \text{mH}$ . The waveforms obtained are shown in Fig. 17(a), which again, are stable since the closed-loop output admittance  $G_{c2}$  in Fig. 4 has been designed to be always passive, as guaranteed by (15). This robustness will obviously be lost in Fig. 17(b) for Case II, since the chosen  $C_g$  and  $L_g$  have caused



(a)



(b)

Fig. 17. Experimental voltage across  $LC$  trap and grid currents with the same  $L_g = 1.2\text{mH}$  and  $C_g = 6.7\ \mu\text{F}$ , but different filter parameters from (a) Case I and (b) Case II.

its resonance peak  $f_r$  to move between  $f_{rc}$  and  $f_s / 6$ . It is therefore important to design with (15) in mind, if robust passivity of  $G_{c2}$  and stability of the system are to be ensured simultaneously.

## VI. CONCLUSION

This paper applies the concept of passivity to an LLCL-filtered converter with the purpose being to derive an optimal condition, which when met, will guarantee system stability and robustness simultaneously. The condition is next extended to include resonance consideration, which when satisfied, will ensure robust stability even with no damping added to the system. Switching harmonic attenuation of the filter will also not be compromised because of the presence of the series LC trap tuned at the switching frequency. The developed criterion is eventually used to improve the filter design procedure with both grid and filter parameter variations taken into consideration. The improved procedure has been tested in the laboratory by using it to design an LLCL-filter for tying a 5-kW converter to the grid. Experimental results obtained show the system remains stable regardless of how the grid impedance changes. Such robustness is no doubt attributed to the optimal criterion developed in the paper.

## REFERENCES

- [1] F. Blaabjerg, R. Teodorescu, M. Liserre, and A. Timbus, "Overview of control and grid synchronization for distributed power generation systems," *IEEE Trans. Ind. Electron.*, vol. 53, no. 5, pp. 1398–1409, Oct. 2006.
- [2] D. Pan, X. Ruan, C. Bao, W. Li, and X. Wang, "Capacitor-current feedback active damping with reduced computation delay for improving robustness of LCL-type grid-connected inverter," *IEEE Trans. Power Electron.*, vol. 29, no. 7, pp. 3414–3427, Jul. 2014.
- [3] M. Liserre, F. Blaabjerg, and S. Hansen, "Design and control of an LCL-filter-based three-phase active rectifier," *IEEE Trans. Ind. Appl.*, vol. 41, pp. 1281–1291, Sep-Oct. 2005.
- [4] M. Huang, W. Wu, Y. Yang, and F. Blaabjerg, "Step by Step Design of a High Order Power Filter for Three-Phase Three-Wire Grid-connected Inverter in Renewable Energy System" in *Proc. PEDG*, 2013, pp.1-8.
- [5] K. Dai, K. Duan, X. Wang, and Yong Kang "Application of an LLCL Filter on Three-Phase Three-Wire Shunt Active Power Filter," in *Proc. IEEE INTELEC*, Sep. 2012, pp. 1-5.
- [6] W. Wu, Y. He, and F. Blaabjerg, "An LLCL power filter for single-phase grid-tied inverter," *IEEE Trans. Power Electron.*, vol. 27, no. 2, pp. 782–789, Feb. 2012.
- [7] M. Huang, P. C. Loh, W. Wu and F. Blaabjerg, "Stability Analysis and Active Damping for LLCL-filter Based Grid-Connected Inverters," in *Proc. IPEC*, 2014, pp. 2610–2617.
- [8] M. Huang, X. Wang, P.C. Loh, and F. Blaabjerg, "Active Damping of LLCL-Filter Resonance Based on LC-Trap Voltage or Current Feedback," *IEEE Trans. Power Electron.*, in press.
- [9] J. M. Bloemink, T C. Green, "Reducing Passive Filter Sizes with Tuned Traps for Distribution Level Power Electronics," in *Proc. IEEE EPE*, Aug. 2011, pp. 1-9.
- [10] S. Parker, B. McGrath, and D.G. Holmes. "Regions of Active Damping Control for LCL Filters," *IEEE Trans. Power Electron.*, vol. 50, no. 1, pp.424-432, Jan. 2014.
- [11] C. Zou, B. Liu, S. Duan, and R. Li, "Influence of Delay on System Stability and Delay Optimization of Grid- Connected Inverters with LCL Filter," *IEEE Trans. Ind. Info.*, vol. 10, no. 3, pp.1775-1784, Aug. 2014.
- [12] X. Wang, F. Blaabjerg, P. C. Loh, "Virtual RC damping of LCL-filtered voltage source converters with extended selective harmonic compensation," *IEEE Trans. Power Electron.*, vol. 30, no. 9, pp.4726-4737, Sep. 2015.
- [13] X. Wang, F. Blaabjerg, P. C. Loh, "Grid-Current-Feedback Active Damping for LCL Resonance in Grid-Connected Voltage Source Converters," *IEEE Trans. Power Electron.*, early access.
- [14] M. Huang, X. Wang, P. C. Loh, and F. Blaabjerg, "Resonant-inductor-voltage feedback active damping based control for grid-connected inverters with LLCL-filters", in *Proc. of ECCE*, 2014, pp. 1194-1201.
- [15] W. Wu, Y. He, T. Tang, and F. Blaabjerg, "A New Design Method for the Passive Damped LCL and LLCL Filter-Based Single-Phase Grid-Tied Inverter," *IEEE Trans. Ind. Electron.*, vol. 60, pp. 4339-4350, Oct. 2013.
- [16] P. Channegowda and V. John, "Filter optimization for grid interactive voltage source inverters," *IEEE Trans. Ind. Electron.*, vol. 57, no. 12, pp. 4106–4114, Dec. 2010.
- [17] S. Zhang, S. Jiang, X. Lu, B. Ge, and F. Z. Peng, "Resonance issues and damping techniques for grid-connected inverters with long transmission cable," *IEEE Trans. Power Electron.*, vol. 29, no. 1, pp.110-120, Jan. 2014.
- [18] O. Brune, "Synthesis of a finite two-terminal network whose driving-point impedance is a prescribed function of frequency," *MIT, Journ. Math. Phys.* vol. 10, pp. 191-236, 1931.
- [19] X. Wang, F. Blaabjerg, and W. Wu, "Modeling and analysis of harmonic stability in an AC power-electronics-based power system," *IEEE Trans. Power Electron.*, vol. 29, no. 12, pp. 6421-6432, Aug. 2014.
- [20] X. Wang, F. Blaabjerg, and P. C. Loh, "Proportional derivative based stabilizing control of paralleled grid converters with cables in renewable power plants," in *Proc. ECCE* 2014, 4917-4924, 2014.
- [21] G. Gohil, L. Bede, R. Teodorescu, T. Kerekes, F. Blaabjerg, "Line Filter Design of Parallel Interleaved VSCs for High Power Wind Energy Conversion Systems," *IEEE Trans. Power Electron.*, early access, 2015.
- [22] A. Riccobono and E. Santi, "A novel passivity-based stability criterion (PBSC) for switching converter DC distribution systems," in *Proc. IEEE APEC* 2012, pp. 2560-2567.
- [23] Robert Meyer, and Axel Mertens, "Design of LCL Filters in Consideration of Parameter Variations for Grid-Connected Converters," in *Proc. IEEE ECCE* 2012, pp. 557-564.
- [24] A. A. Rockhill, M. Liserre, R. Teodorescu and P. Rodriguez, "Grid-Filter Design for a Multimegawatt Medium-Voltage Voltage-Source Inverter," *IEEE Trans. Ind. Electron.*, vol. 58, no. 4, pp. 1205-1217, Apr. 2011.
- [25] J. Yang, F.C. Lee, "LCL Filter Design and Inductor Current Ripple Analysis for 3-level NPC Grid Interface Converter," *IEEE Trans. Power Electron.*, vol. 30, no. 9, pp. 4659-4668, Sep. 2015.
- [26] Q. Liu, L. Peng, Y. Kang, S. Y. Tang, D. L. Wu, and Y. Qi, "A Novel Design and Optimization Method of an LCL Filter for a Shunt Active Power Filter," *IEEE Trans. Ind. Electron.*, vol. 61, pp. 4000-4010, Aug. 2014.
- [27] J. Xu, J. Yang, J. Ye, Z. Zhang, A. Shen, "An LTCL Filter for Three-Phase Grid-Connected Converters," *IEEE Trans. Power Electron.*, vol. 29, no. 8, pp.4322-4338, Aug. 2014.
- [28] J. K. Phipps, "A transfer function approach to harmonic filter design," *IEEE Ind. Appl. Mag.*, vol. 3, no. 2, pp. 68–82, Mar./Apr. 1997.
- [29] *IEEE Recommended Practices and Requirements for Harmonic Control in Electrical Power Systems*, IEEE Standard 519-1992, 1992.
- [30] J.C. Das, "Passive Filters—Potentialities and Limitations," *IEEE Trans. Power Electron.*, vol. 40, no. 1, pp. 232–241, Jan./Feb. 2014.